Journal of Musculoskeletal and Neuronal Interactions JMNI

Original Article

Characterization and Biocompatibility Assessment of 3D-Printed HA/PCL Porous Bionic Bone Scaffold: *in Vitro* and *in Vivo* Evaluation

Shi Shen#[1], Benchao Shu#[1,2], Yulin Xu[1], Heng Zhao[1], Yang Li[1], Yujie Li[1], Chuanchuan Zhuo[1], Naiqiang Zhuo[1]

[1]Department of Bone and Joint Surgery, The Affiliated Hospital of Southwest Medical University, Luzhou, Sichuan, China;
[2]Department of Joint Trauma Surgery, Guangyuan First People's Hospital, Guangyuan, Sichuan, China.
#Equal Contribution

Abstract

Objectives: This study aims to characterize a three-dimensional-printed hydroxyapatite (HA)/polycaprolactone (PCL) scaffold and assess its biocompatibility both *in vitro* and *in vivo*. **Methods**: A bionic, porous HA/PCL scaffold was fabricated using 3D printing, and its microstructure, porosity, hydrophilicity, and mechanical properties were evaluated through scanning electron microscopy and various assays. Bone marrow mesenchymal stem cells (BMSCs) and vascular endothelial progenitor cells (VEPCs) were co-cultured with the scaffold, and their proliferation and osteogenic differentiation were assessed using the Cell Counting Kit-8, ALP assays, and alizarin red staining. Osteogenic marker expression was analyzed via qRT-PCR. In vivo bone regeneration was evaluated through histological analysis of H&E and Masson's trichrome staining in a rat cranial defect model. **Results**: The average pore size of the scaffold was 462.00 ± 100.389 μm, with a porosity of 53%, a water absorption expansion rate of 5.10%, a contact angle of 94.55°, an elastic modulus of 53.82 MPa, and a compressive strength of 6.10 MPa. ALP activity and qRT-PCR analysis of osteogenic markers (BMP2, OCN, Runx2) showed significant upregulation in cells co-cultured with the scaffolds. *In vivo* experiments demonstrated enhanced bone regeneration and collagen deposition in the HA/PCL scaffold group. **Conclusion**: The results suggest that the HA/PCL scaffold promotes osteogenic differentiation and bone regeneration, making it suitable for bone tissue engineering applications.

Keywords: Bionic Bone Scaffolds, Bone Tissue Engineering, Osteogenic Differentiation, Seed Cells, Three-Dimensional Printing

Introduction

Large segment bone defects can arise from various causes, such as severe trauma, infection, chronic osteomyelitis, bone tumor surgery, and congenital malformations. Moreover, their incidence is steadily increasing each year[1,2]. The healing of bone defects is further complicated by factors such as insufficient blood supply to the defect area, infection, and tumors, making self-repair of the defects difficult[3]. Approximately 2 million bone grafting procedures are performed annually worldwide, making bone the second most transplanted tissue after blood transfusions[2]. However, bone transport presents challenges, including prolonged treatment cycles, joint stiffness, muscle atrophy, and inconvenience caused by the use of large external fixators[4]. Membrane induction technology also introduces issues such as extensive trauma, long treatment durations, difficulties in sourcing adequate bone material, and secondary trauma[5]. As a result, the development of bone grafts and substitutes for treating bone defects has become a prominent area of research.

Currently, three-dimensional (3D) printing in bone tissue engineering and bone regeneration is gradually emerging, offering new hope for the repair of large segment bone defects. Seed cells are injected into bionic structural bone scaffolds, using tissue engineering scaffolds to form a cell-

The authors have no conflict of interest.

Corresponding author: Naiqiang Zhuo, Department of Bone and Joint Surgery, The Affiliated Hospital of Southwest Medical University, 25 Taiping Street, Jiangyang District, Luzhou 646099, Sichuan, China
E-mail: Znq0101@163.com

Edited by: G. Lyritis
Accepted 21 November 2024

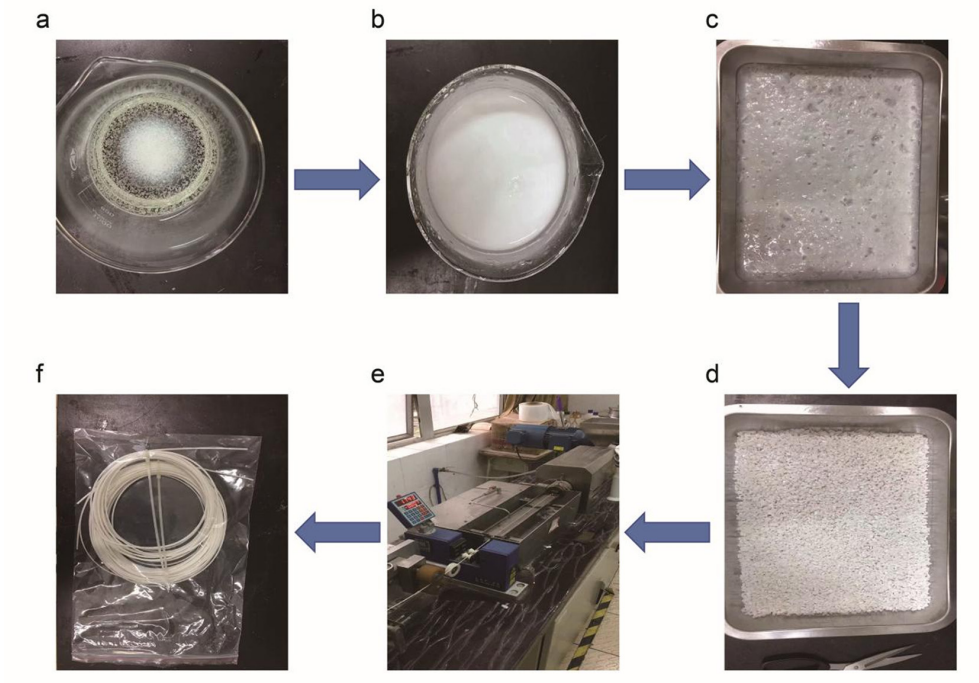

Figure 1. The production procedures of PCL/HA wire: (a) Dissolution of PCL using N,N-dimethylformamide; (b) Addition of HA to the mixture; (c) Vacuum drying; (d) Cutting of the dried material, followed by quick drying; (e) Extrusion of the material into filaments using the machine; (f) PCL/HA wire. PCL, polycaprolactone; HA, hydroxyapatite.

scaffold complex. This complex is then implanted into the bone defect, ultimately achieving the goal of repairing the defect[6,7]. At present, scaffold materials used in bone tissue engineering are mainly categorized into two types: inorganic materials, such as hydroxyapatite and tricalcium phosphate, and organic materials, including natural materials and synthetic degradable polymers like polycaprolactone (PCL)[8]. Human bone is a heterogeneous composite structure[9,10]. Composite materials have been developed to design ideal scaffolds for bone tissue engineering, combining the characteristics and advantages of these materials in a complementary manner. PCL offers good biocompatibility and shape retention, while hydroxyapatite (HA), with its high biological activity, is an ideal bone replacement material[11]. The HA/PCL composite is considered an optimal material for bone scaffolds. Several studies have explored the physicochemical properties and fabrication processes of HA/PCL materials[11-13]. However, the properties of scaffolds produced by different processes vary, and the biocompatibility of HA/PCL materials remains unclear. This study aims to explore the physicochemical properties and biocompatibility of HA/PCL scaffolds.

Materials and Methods

Production of PCL/HA Wire

The HA/PCL 3D bionic porous bone scaffold was fabricated using 3D printing. The HA/PCL composite system was prepared with a mass ratio of 15:85 based on pre-experimental results and previous literature[10]. The overall production process is shown in Figure 1. First, 1 g of PCL was dissolved in 10 mL of N,N-dimethylformamide to create a PCL solution. The appropriate mass ratio of HA was then added to the PCL solution. To enhance biological activity, the solution was supplemented with small amounts of salts, including silicic acid, calcium, sodium, and strontium. The salt ratio was approximately Boron:sodium:phosphorus: silicic acid:calcium = 1:2.1:8.4:9.8:31, with the salt content making up about 1% of the PCL content. The mixture was dissolved at a constant temperature of 70°C and stirred at 500 rpm. After vacuum drying, the material was cut, soaked, and cleaned with deionized water repeatedly. After drying again, the cut particles were extruded to form HA/PCL wire using an extruder (Figure 1 a–f).

Preparation of 3D Printed HA/PCL Scaffold

The interconnected 3D bionic porous scaffold model was designed using Pro/ENGINEER software (Parametric Technology Corporation, Boston, MA, USA). The scaffold model was designed with overall dimensions of 8 mm × 8 mm × 13 mm to match the tibial defect size of New Zealand white rabbits (Figure 2a). The HA/PCL scaffold was then prepared using high-temperature melting deposition and 3D printing (FS-10, Fly Thinking, Guangzhou, China) (Figure

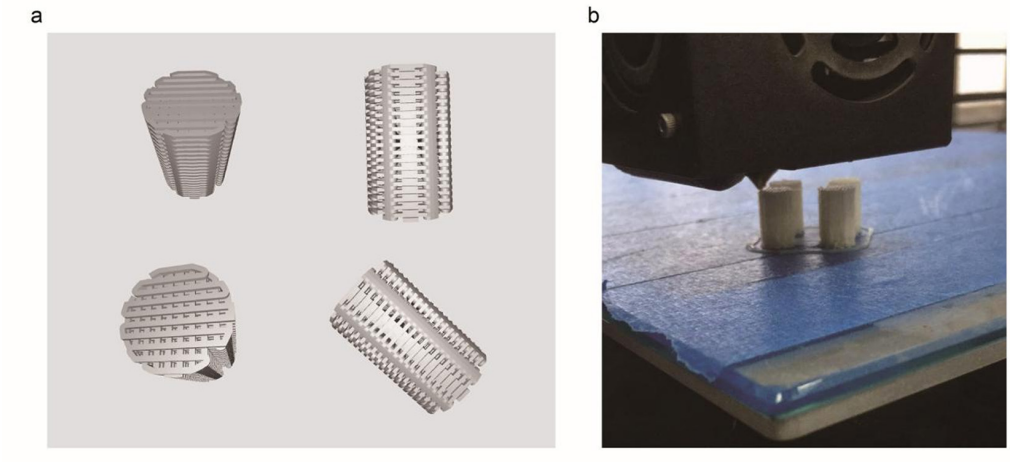

Figure 2. The preparation of 3D printed HA/PCL scaffold: (a) The 3D model diagram of HA/PCL scaffolds; (b) The HA/PCL scaffolds prepared by 3D printing. The melting temperature is approximately 180°C, with a cooling time of about 12 minutes. 3D, three-dimensional; PCL, polycaprolactone; HA, hydroxyapatite.

2b). The microstructure of the scaffold was observed using a scanning electron microscope (SEM; S-4800, Hitachi, Japan). Elemental analysis was also performed using SEM.

The Evaluation of Mechanical and Physicochemical Properties of the Scaffolds

Porosity Measurement

A certain amount of deionized water was placed into a prepared cylinder, and the initial volume (V1) was recorded. Next, the HA/PCL 3D porous bone scaffold (without cells) was immersed for 5 minutes, and the new volume (V2) was recorded. The scaffold was then placed in a vacuum drying oven with negative pressure suction for degassing, allowing the deionized water to fill the scaffold's pores until no bubbles escaped. The volume at this stage (V3) was noted. The porosity (E) was calculated using the formula:
E = (V2 - V3) / (V2 - V1).

The porosity of three samples was measured individually, and the average value was calculated.

Measurement of Water Absorption and Expansion Rate

The HA/PCL 3D bionic porous bone scaffold (without cells) was soaked in deionized water. After soaking at room temperature for 10 minutes, the scaffold was removed. The scaffold was then left in the air for 1 minute until no water droplets remained, after which it was weighed (W). Next, the scaffold was dried in a vacuum drying oven at 30°C for 12 hours and weighed again (WO). Three samples were tested separately, and the average was calculated. The apparent density test method was used for calculation. The formula is as follows:
X = (W - WO) / W

Evaluation of the Hydrophilicity of Scaffold Materials

The hydrophilicity of the material was evaluated by measuring the contact angle. The HA/PCL solution was freeze-dried for 24 hours to obtain HA/PCL samples. The sample was then cut into 10 × 10 × 1 mm square pieces and placed on a slide. The surface of the sample was leveled, and deionized water droplets were applied to the surface using a microinjector equipped with a 27 G blunt needle. The surface contact angle was measured using the NuonaSL-200B Droplet Analysis System (Kono Industries, USA), and the experiment was repeated three times.

Shore Hardness Assessment

The hardness of the scaffold materials was measured using a Shore hardness tester. A Shore hardness of 90 or greater is considered soft plastic, while values below 90 are classified as rubber. The test samples were placed on a hard platform, and the presser foot of the hardness tester was smoothly pressed into the sample with stability, ensuring the foot was parallel to the surface. Sufficient force was applied to ensure complete contact between the presser foot and the sample. The force was recorded within one second after full contact. Five different positions on each sample were tested, and the mean value was calculated. Three samples were tested in total, and the average value was computed.

The Compression Modulus

Three 3D bionic porous bone scaffolds were cut into standard mechanical test specimens. The samples were then fixed onto a mechanical testing machine and compressed at a rate of 2 mm/min. The Young's modulus was calculated based on the stress-strain curve.

Isolation and Identification of Seed Cells

Bone marrow stem cells (BMSCs) were extracted from 4-week-old New Zealand white rabbits provided by the Experimental Animal Center of Southwest Medical University. The rabbits were selected for iliac bone puncture to aspirate bone marrow fluid, which was then loaded into anticoagulant tubes and diluted with phosphate-buffered saline (PBS). The bone marrow mixture was gently added to the upper layer of Percoll separation solution (Solarbio, China), avoiding mixing with the Percoll solution. After centrifugation, the central cell layer (mononuclear cell layer) was gently aspirated. The cell suspension was mixed with an equal volume of PBS and centrifuged again, discarding the supernatant. This washing procedure was repeated twice. After the final centrifugation, the cells were resuspended in 2 mL Dulbecco's Modified Eagle Medium (Corning, USA) containing 10% fetal bovine serum (HyClone, USA). The cell suspension was then inoculated into a 25 cm^2 culture flask, followed by the addition of 5 mL of medium. After 48 hours, the medium was replaced, and the cells were incubated in a humidified incubator at 37°C with 5% CO_2.

Vascular endothelial progenitor cells (VEPCs) were isolated from bone marrow cell suspension by repeatedly washing the cancellous bone and medullary cavity of 4-week-old New Zealand white rabbits. The bone marrow cell suspension was carefully layered onto the surface of Percoll solution (density 1.083). After centrifugation, the cell pellet (cell cloud) was collected and washed. The cells were then cultured in medium containing 1 μg/mL vascular endothelial growth factor (VEGF), 1 μg/mL basic fibroblast growth factor (bFGF), 10 ng/mL epidermal growth factor (EGF), 1 mg/mL hydrocortisone, 100 U/mL penicillin, and 100 U/mL streptomycin.

The isolated cells (BMSCs and VEPCs) were identified using immunofluorescence assay. Cells were fixed with paraformaldehyde at 4°C for 30 minutes. After washing with PBS, the cells were incubated with primary antibodies overnight at 4°C. The primary antibodies used were CD44 (60224-1-1g, 1:100, Proteintech) and CD31 (66065-2-1g, 1:100, Proteintech). After rinsing, secondary antibody incubation was performed at room temperature for 2 hours. The cell nucleus was stained with 4',6-diamidino-2-phenylindole (DAPI) for 5 minutes. The cells were observed using a TCS SP8 confocal microscope (Leica, Germany).

Cell Treatment

The isolated cells were subcultured in appropriate medium. The second-generation cells (BMSCs and VEPCs) were used for the experiments. The cells were prepared as a single-cell suspension at a concentration of 1×10^6 cells/mL. The cells were divided into five experimental groups:

- (Groups 1–2) 100 μL of BMSCs or VEPCs suspension was added to culture dishes for cultivation, respectively.
- (Groups 3–4) HA/PCL scaffold materials were supplemented with 100 μL of BMSCs or VEPCs suspension, respectively.
- (Group 5) HA/PCL scaffolds were added with 100 μL of cell suspension, which contained 50 μL of BMSCs and 50 μL of VEPCs cell suspension.

Cell morphology was photographed at 6 hours, 7 days, and 14 days. Cell proliferation was assessed using the Cell Counting Kit-8 (CCK-8) assay at 24 and 48 hours. Specifically, CCK-8 solution (Tongren Company, Japan) was added to the culture dish, and the cells were incubated for 1.5 hours. The optical density at 450 nm was then measured.

ALP

Alkaline phosphatase (ALP) activity was measured using an ALP assay kit (Nanjing Jiancheng Bioengineering Institute, Nanjing, China, Cat. No. A059-2). Cells from the following groups were harvested: BMSCs, BMSCs + scaffolds, combined BMSCs and VEPCs + scaffolds, VEPCs, and VEPCs + scaffolds. ALP activity was quantified according to the manufacturer's instructions. Absorbance was measured at 405 nm using a microplate reader (Thermo Fisher Scientific, Waltham, MA, USA), and ALP levels were expressed in IU/L, based on a standard curve generated from the kit.

Alizarin Red Staining

Cells were cultured according to the designated groupings and treated with an inducer. Alizarin red staining was performed after 14 days. Briefly, the cells were fixed with 4% paraformaldehyde for 20 minutes at room temperature and then washed with PBS. Alizarin red staining (Solarbio, China) was applied for incubation at room temperature for approximately 10 minutes. The cells were then rinsed with PBS and observed under a microscope. The pixel grayscale of the alizarin red-positive area was extracted using Image J (version 1.8.0, NIH, Bethesda, MD, USA), and the average grayscale value of the positive area was semi-quantitatively calculated.

Animal Model and Surgical Procedures

Six male Sprague-Dawley (SD) rats (n=3 per group), aged 6–8 months and weighing approximately 300–350 g, were obtained from the Laboratory Animal Center of Sichuan Provincial People's Hospital (Chengdu, China). The animals were housed under standard laboratory conditions, including a 12-hour light/dark cycle, controlled temperature (22°C), and humidity (50–60%), with free access to food and water.

For both the PCL and HA/PCL groups, rats were anesthetized with 2% isoflurane (RWD Life Science Co., Ltd., Shenzhen, China) in an induction chamber. The skin overlying the parietal bone was shaved and sterilized with povidone-iodine. A midline incision was made to expose the parietal bone, and two bilateral cranial defects, each with a diameter of 4 mm, were created using a dental drill (NSK Ultimate XL-K, Japan). To fit the cranial defect model, the original 3D-printed scaffolds (dimensions: 8 mm × 8 mm × 13 mm) were trimmed into cylindrical pieces measuring approximately 4 mm in diameter and 2 mm in thickness. These trimmed scaffolds ensured

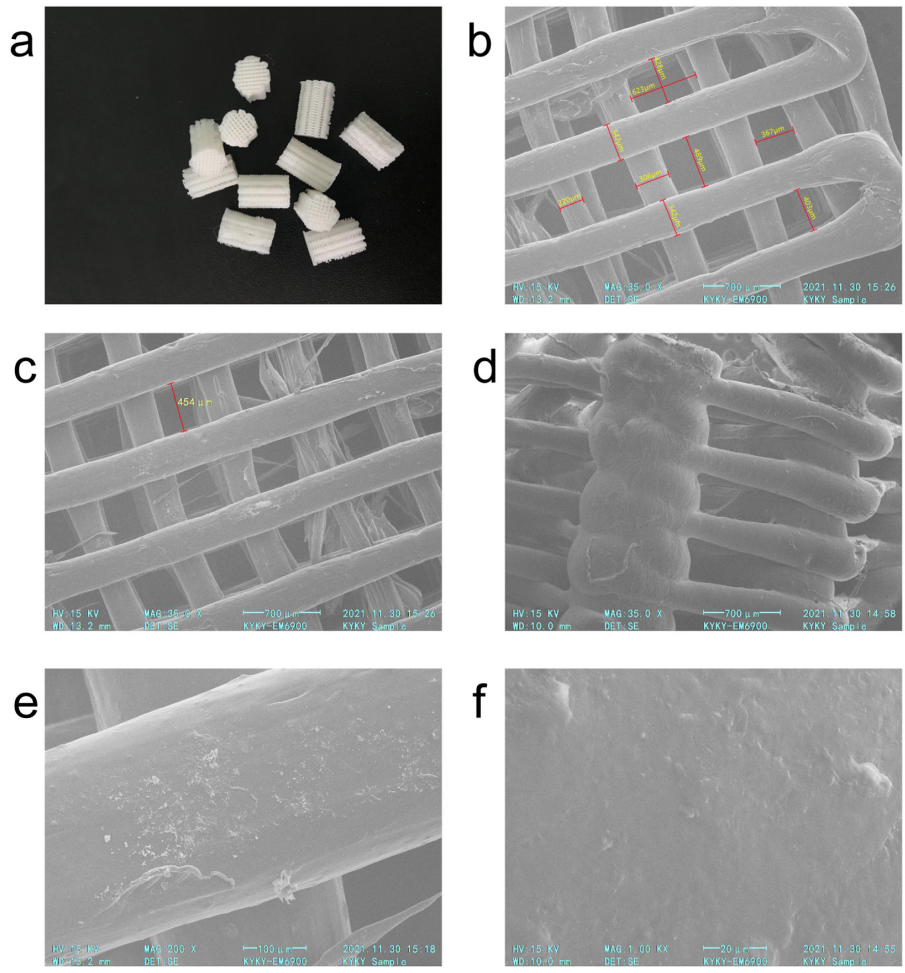

Figure 3. The microstructure of the HA/PCL scaffold: (a) The general appearance of the 3D-printed HA/PCL scaffold; (b) The microstructure of the HA/PCL 3D bionic porous bone scaffold observed using SEM (35.0×), with pore size and fiber bundle size measured. The pore size of the scaffold was measured using SEM, and the average pore size was calculated by repeating the measurement five times. (c–d) The microstructure of the scaffold observed using SEM (35×), showing rectangular micropores with connections in all vertical directions and good connections in horizontal directions. (e–f) Calcium salts on the surface of the cylindrical fibers under SEM (Figure e: 200×, Figure f: 1000×). 3D, three-dimensional; SEM, scanning electron microscope; HA, hydroxyapatite; PCL, polycaprolactone.

proper coverage of the defect area. In the PCL group, a 3D-printed polycaprolactone (PCL) scaffold, prepared from polycaprolactone filament (Sigma-Aldrich, St. Louis, MO, USA), was implanted into the defects. In the HA/PCL group, the defects were filled with a 3D-printed hydroxyapatite/polycaprolactone (HA/PCL) scaffold, fabricated from HA powder (Alfa Aesar, Thermo Fisher Scientific, USA) and PCL filament (Sigma-Aldrich, USA). After scaffold implantation, the skin was sutured with 4-0 nylon sutures (Ethicon, Inc., Johnson & Johnson, USA). Postoperatively, all rats received meloxicam (5 mg/kg, Boehringer Ingelheim, Germany) for analgesia and were monitored daily for signs of infection or discomfort.

PCR

Total RNA was extracted from the cell groups (BMSCs, BMSCs + scaffolds, VEPCs, VEPCs + scaffolds, and combined cell + scaffolds group) and cranial bone tissues from the PCL and HA/PCL groups at 8 weeks post-implantation. RNA extraction was performed using TRIzol reagent (Thermo Fisher Scientific, Cat. No. 15596018), and reverse transcription was carried out using PrimeScript RT Master Mix (Takara, Dalian, China, Cat. No. RR036A). Quantitative RT-PCR (qRT-PCR) was performed using the TB Green Premix Ex Taq II (Takara, Cat. No. RR820A) on a Bio-Rad CFX96 Real-Time PCR Detection System (Bio-Rad, Hercules, CA, USA) to assess the expression levels of osteogenic markers, including BMP2, OCN, and Runx2.

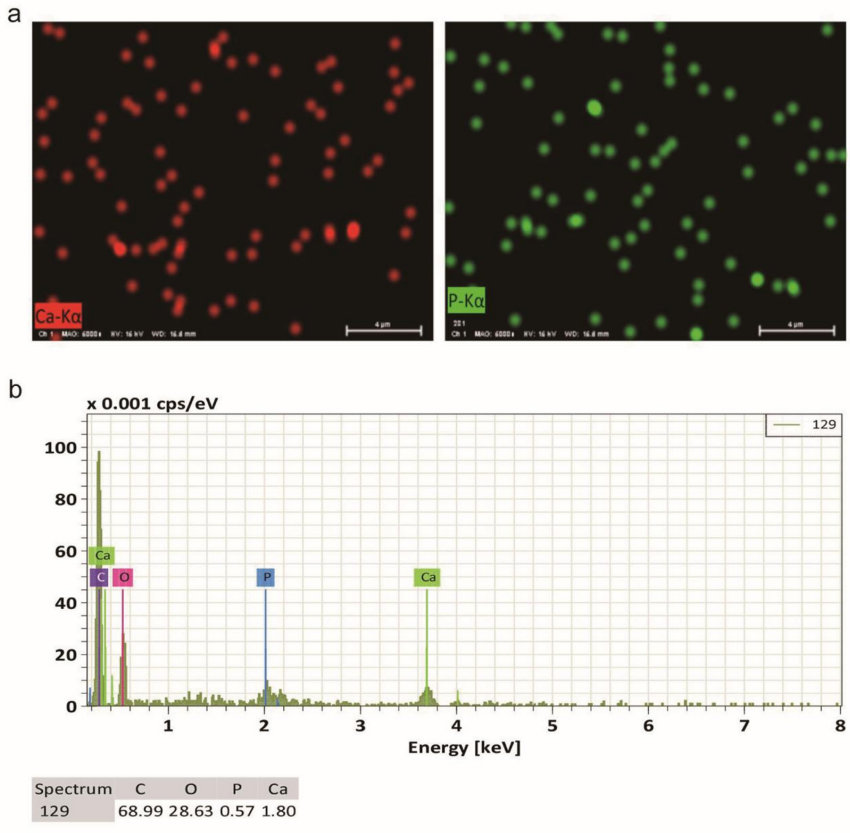

Figure 4. Elemental analysis of the scaffold material: (a) The energy spectrum distribution of Ca and P analyzed by SEM; (b) The distribution of elements (C, O, P, Ca) analyzed in the scaffold material by SEM. Ca, calcium; P, phosphorus; SEM, scanning electron microscope; C, carbon; O, oxygen.

Table 1. The physicochemical properties of scaffolds in three samples.

Characterization	Porosity	Thickness swelling rate	Contact Angle	Shore hardness	Young's modulus	Compressive strength
Sample a	49%	4.57%	105.7°	78.2 HA	47.67 MPa	6.05 MPa
Sample b	56%	5.07%	83.26°	80 HA	46.98 MPa	4.74 MPa
Sample c	54%	5.66%	94.68°	76.6 HA	69.82 MPa	7.52 MPa
Mean value	53%	5.10%	94.55°	78.27 HA	53.82 MPa	6.10 MPa

GAPDH was used as the internal control, and relative gene expression levels were calculated using the 2^-ΔΔCt method. Primer sequences for each gene were as follows: BMP2 (forward: 5′-ACCCGCTGTCTTCTAGTGTTG-3′, reverse: 5′-CAACTCAAACTCGCTGAGGAC-3′), OCN (forward: 5′-CCACCGTTTAGGGCATGTGT-3′, reverse: 5′-AGCTGTGCCGTCCATACTTT-3′), and Runx2 (forward: 5′-CACAAGTGCGGTGCAAACTT-3′, reverse: 5′-ATGACTCGGTTGGTCTCGGT-3′).

HE Staining

Cranial bone tissues from both the PCL and HA/PCL groups were harvested at 8 weeks post-surgery for histological analysis. The tissues were fixed in 10% neutral-buffered formalin (Sinopharm Chemical Reagent Co., Ltd., Shanghai, China), decalcified in 10% EDTA (Sigma-Aldrich, USA), and embedded in paraffin. Serial sections (5 μm) were cut using a microtome (Leica

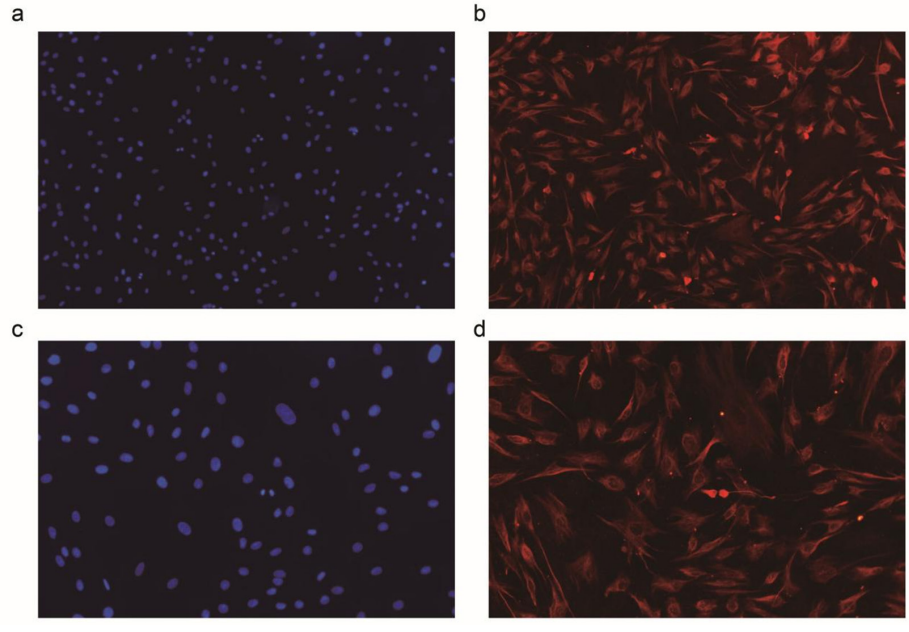

Figure 5. The identification of BMSCs using CD44 immunofluorescence staining (a–b: 100X; c–d: 200X). DAPI was used for nucleus staining (blue), and CD44 for BMSCs staining (red). BMSCs, bone marrow stem cells; DAPI, 4',6-diamidino-2-phenylindole.

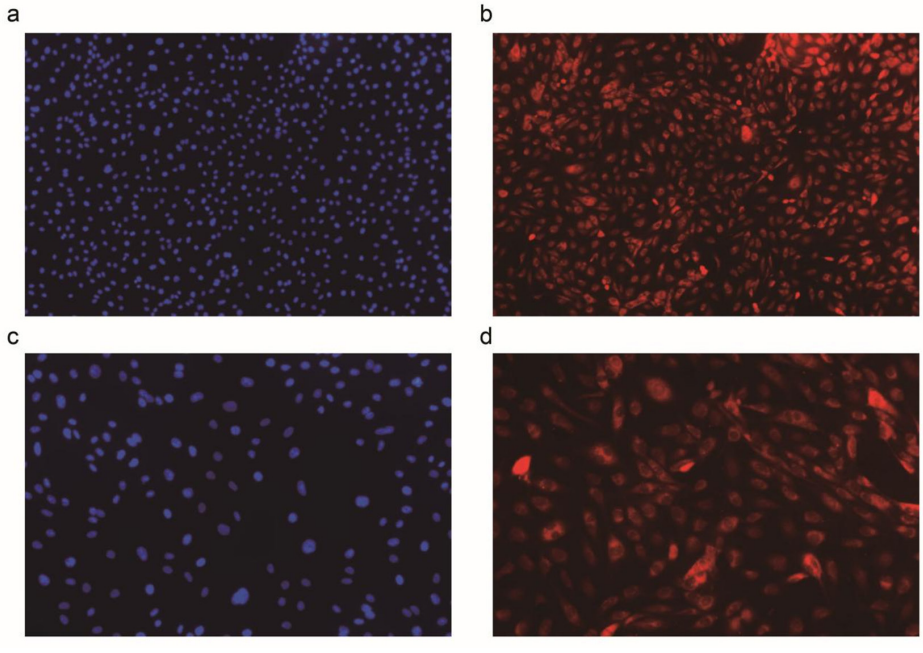

Figure 6. The identification of VEPCs using CD31 immunofluorescence staining (a–b: 100X; c–d: 200X). DAPI was used for nucleus staining (blue), and CD31 for VEPCs staining (red). VEPCs, vascular endothelial progenitor cells; DAPI, 4',6-diamidino-2-phenylindole.

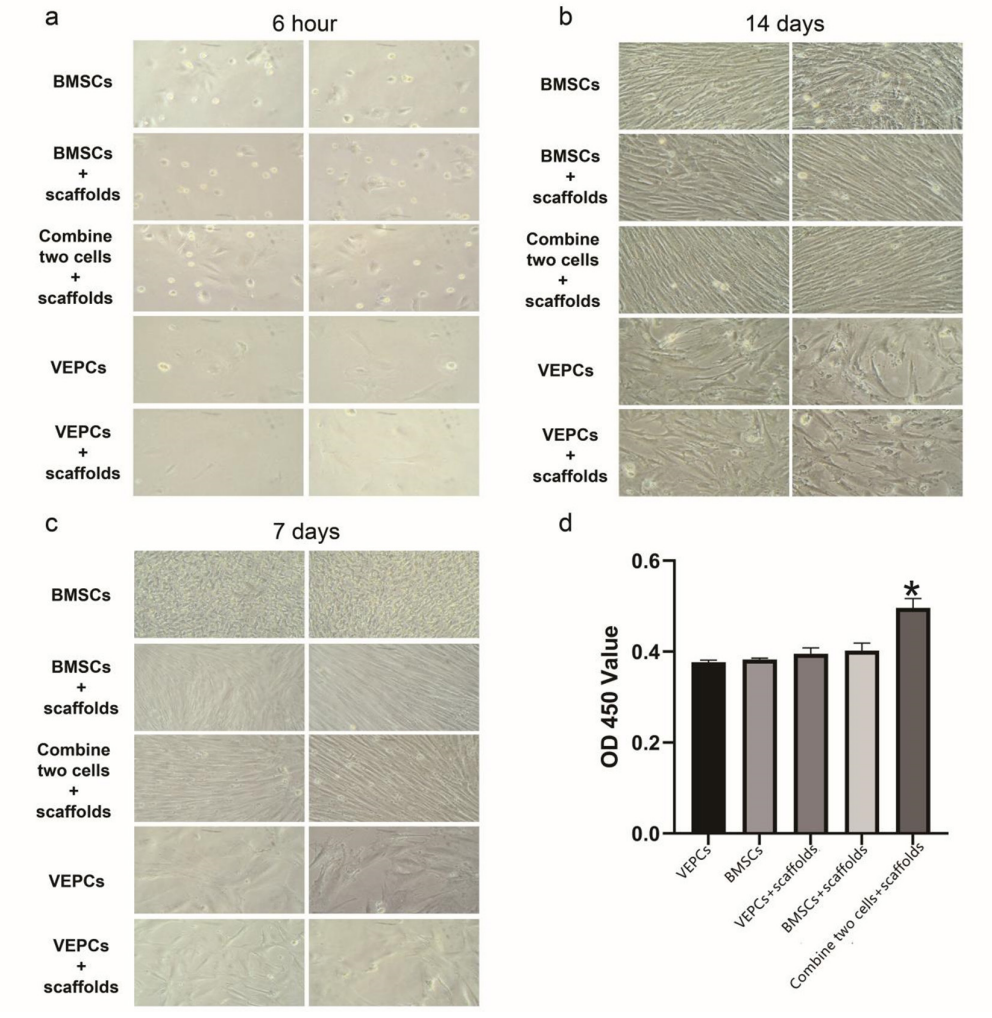

Figure 7. The effects of scaffold materials on cell morphology of BMSCs and VEPCs. (a–c) Measurement of cell morphology of BMSCs and VEPCs at 6 h (a), 7 d (b), and 14 d (c). (d) Detection of cell viability using CCK-8. *P < 0.05 vs. other groups. BMSCs, bone marrow stem cells; VEPCs, vascular endothelial progenitor cells; CCK-8, Cell Counting Kit-8. The experiment was repeated three times.

RM2235, Leica Biosystems, Germany) and stained with hematoxylin and eosin (H&E) (Beyotime Biotechnology, Shanghai, China, Cat. No. C0105). The stained sections were examined under a light microscope (Olympus BX53, Olympus Corporation, Tokyo, Japan) to evaluate the extent of new bone formation and scaffold integration.

Masson Trichrome Staining

Paraffin-embedded tissue sections were stained using a Masson trichrome staining kit (Solarbio Life Sciences, Beijing, China, Cat. No. G1340) following the manufacturer's instructions. This staining differentiates collagen fibers (stained blue), newly formed bone (stained red), and cells (stained black or dark brown). After staining, the sections were examined under a light microscope (Olympus BX53, Olympus Corporation, Tokyo, Japan) at 100× and 400×, and the degree of collagen deposition and bone matrix formation was qualitatively assessed.

Statistical Analysis

Statistical analysis was performed using SPSS 17.0 (Chicago, IL, USA), and GraphPad Prism (San Diego, CA, USA) was used for plotting. Data are presented as mean ± standard deviation. An independent sample t-test was used for comparisons between two groups. A one-way analysis of variance (ANOVA) was employed to compare differences among multiple groups, and the Bonferroni test was used as a post hoc analysis. A p-value of < 0.05 was considered statistically significant.

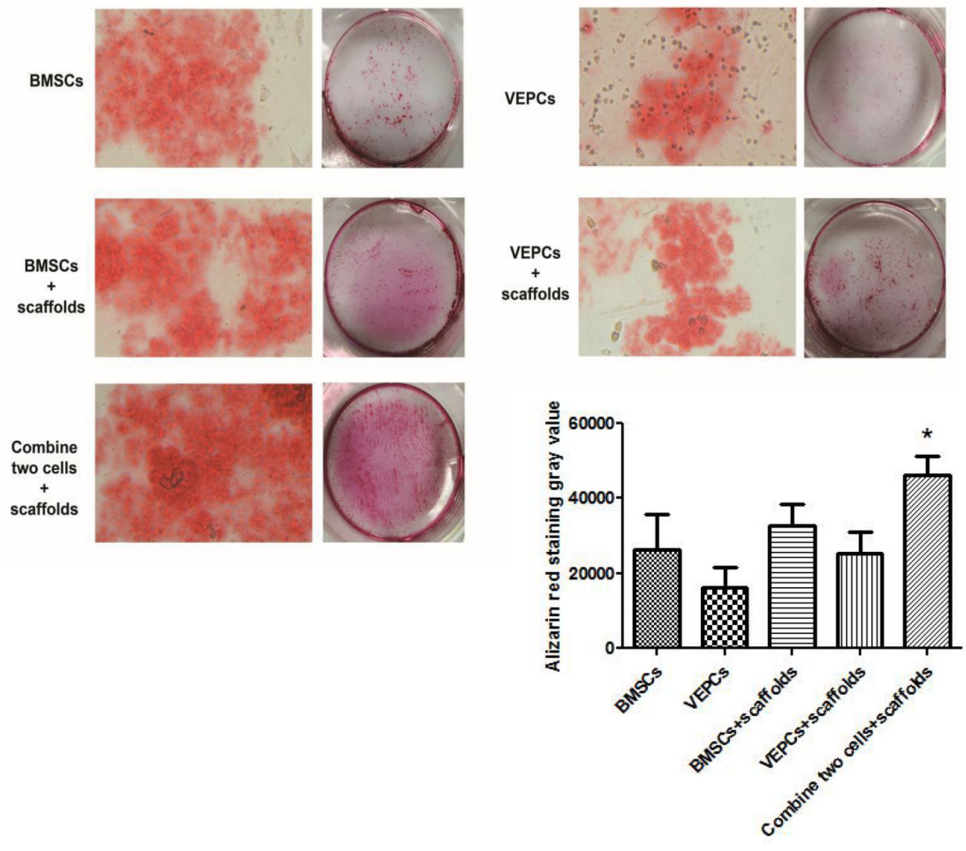

Figure 8. The assessment of osteogenic differentiation ability of cells by Alizarin Red staining. *P < 0.05 indicates comparison with other groups. The experiment was repeated three times.

Results

Scaffold Morphology and Microstructure

The morphology of the scaffold was first observed. The HA/PCL bionic scaffold exhibited an interconnected porous structure (Figure 3a). Scanning electron microscopy (SEM) revealed pores on the surface of the scaffold and interconnected pores on the sides. The average pore size of the HA/PCL scaffold was 462.00 ± 100.389 μm (Figure 3b). The fibers were neatly arranged and tightly connected (Figures 3c–f).

Elemental Analysis

The elemental content of the 3D porous scaffold was analyzed using SEM energy spectroscopy. The energy spectrum distribution of calcium and phosphorus was measured (Figure 4a). The elemental distribution map showed that the total content of carbon, oxygen, phosphorus, and calcium was 99.99%, while the content of silicon (Si) and strontium (Sr) was 0.01% (Figure 4b).

Characterization of Physicochemical Properties of Scaffolds

The physicochemical properties of the scaffolds were evaluated, and the characterization results are shown in Table 1. The scaffolds demonstrated good porosity, water absorption and expansion rate, and compressive strength. However, some deficiencies in hydrophilicity and Shore hardness were observed. Overall, the physicochemical properties of the scaffolds were well aligned with those of human cancellous bone.

Identification of Seed Cells

BMSCs and VEPCs were isolated from rabbits, and the seed cells were identified by immunofluorescence. CD44 was expressed in BMSCs (Figure 5), and CD31 was expressed in VEPCs (Figure 6). These results confirmed the successful isolation of primary BMSCs and VEPCs.

Biocompatibility of Scaffold Materials

To assess the biocompatibility of the scaffold materials, BMSCs and VEPCs were separately or simultaneously loaded

Figure 9. ALP activity and the expression levels of osteogenic markers (BMP2, OCN, and Runx2) in different experimental groups. The graph shows ALP activity (a) and the relative expression of BMP2, OCN, and Runx2 (b) as determined by qRT-PCR. The experiment was repeated three times. P < 0.01 vs. BMSCs group (**); P < 0.01 vs. VEPCs group (##).

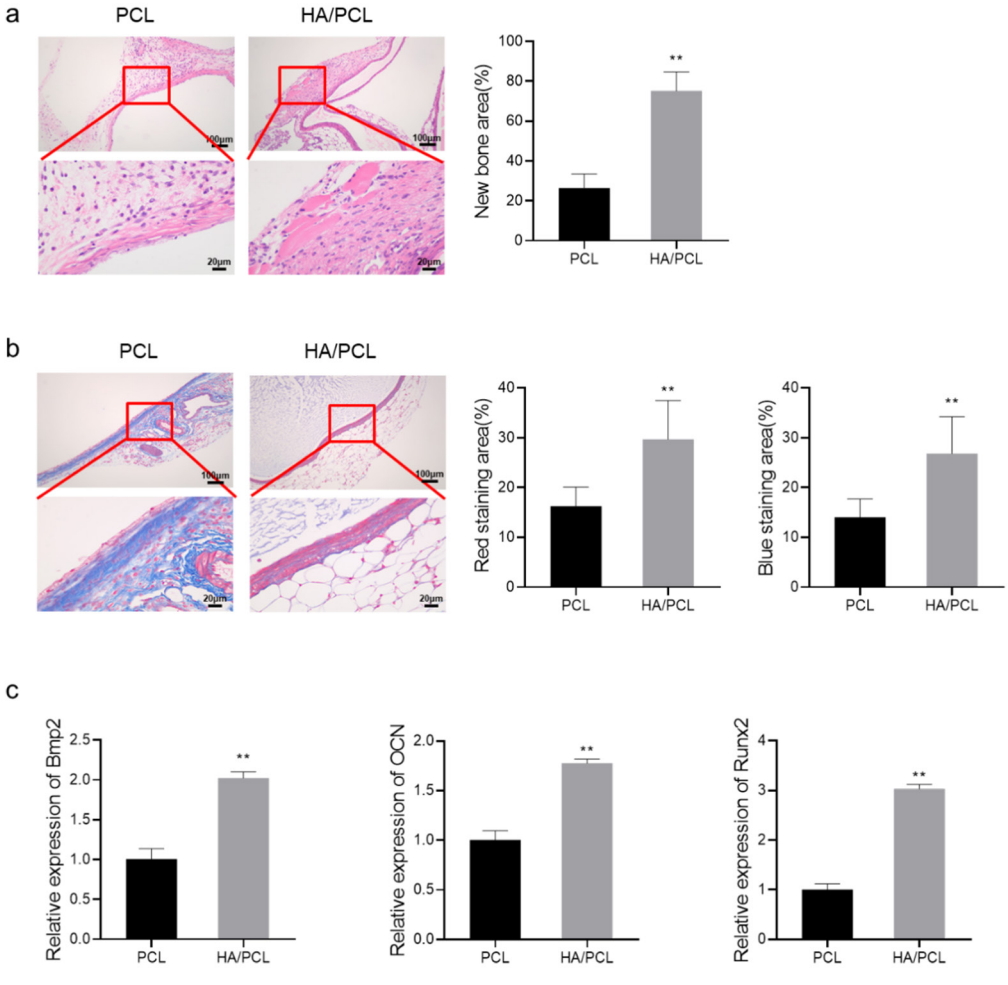

Figure 10. Histological and qRT-PCR analysis of cranial bone tissue from the PCL and HA/PCL groups. (a) H&E staining of cranial bone tissue at 8 weeks post-surgery. Scale bars: 100 μm and 20 μm. (b) Masson's trichrome staining of cranial bone tissue. Scale bars: 100 μm and 20 μm. (c) The relative expression levels of osteogenic markers in cranial bone tissue from the PCL and HA/PCL groups. P < 0.01 vs. PCL group (**).

onto the scaffolds. Cell morphology was observed at 6 h, 7 d, and 14 d (Figure 7a–c). The CCK-8 assay results showed that the scaffold materials exhibited no cytotoxicity towards BMSCs and VEPCs. The combined loading of BMSCs and VEPCs promoted cell proliferation ($P < 0.05$, Figure 7d). Alizarin red staining was used to evaluate the osteogenic differentiation of the cells. The results indicated that, compared to the groups with BMSCs or VEPCs alone, cells co-cultured with scaffold materials demonstrated enhanced osteogenic differentiation. Specifically, the mixed-cell culture co-cultured with the scaffold materials exhibited the most pronounced osteogenic differentiation ability among all groups (Figure 8).

ALP Activity and Expression of Osteogenic Markers

The ALP activity levels in the different experimental groups are shown in Figure 9a. The BMSCs + scaffolds group exhibited a significant increase in ALP levels compared to the BMSCs group ($P < 0.01$). Similarly, the VEPCs + scaffolds group showed significantly higher ALP levels than the VEPCs group ($P < 0.01$). Although the BMSCs group had slightly higher ALP activity than the VEPCs group, this difference was not statistically significant. The BMSCs + scaffolds group also showed slightly higher ALP levels than the VEPCs + scaffolds group. Notably, the combined BMSCs and VEPCs + scaffolds group demonstrated significantly higher ALP activity than all other groups ($P < 0.01$), suggesting a synergistic enhancement of osteogenic differentiation when both cell types were combined.

The expression levels of osteogenic markers (BMP2, OCN, and Runx2) were assessed using qRT-PCR (Figure 9b). In the BMSCs + scaffolds group, the expression of BMP2, OCN, and Runx2 was significantly elevated compared to the BMSCs group ($P < 0.01$). Similarly, the VEPCs + scaffolds group showed a significant increase in the expression of these markers compared to the VEPCs group ($P < 0.01$). While the BMSCs group showed slightly higher expression of BMP2, OCN, and Runx2 than the VEPCs group, the BMSCs + scaffolds group demonstrated slightly higher expression of these genes than the VEPCs + scaffolds group. Importantly, the combined BMSCs and VEPCs + scaffolds group exhibited significantly higher levels of BMP2, OCN, and Runx2 compared to all other groups ($P < 0.01$), indicating a robust osteogenic response.

In Vivo Bone Regeneration and Osteogenic Marker Expression

H&E staining results revealed differences in new bone formation between the PCL and HA/PCL groups. In the PCL group, only a small amount of new bone tissue was observed within the defect area, indicating limited bone regeneration. In contrast, the HA/PCL group exhibited significantly more newly formed bone tissue, although the bone defect was not fully regenerated. The HA/PCL scaffolds promoted substantially greater new bone formation compared to the PCL group, suggesting that the addition of hydroxyapatite enhances bone regeneration ($P < 0.01$, Figure 10a).

Masson's trichrome staining showed a clear distinction in collagen fiber deposition between the two groups. In the PCL group, soft connective tissue was visible, with minimal collagen formation. In comparison, the HA/PCL group demonstrated significantly more mature collagen fibers, indicating enhanced tissue remodeling and bone matrix maturation. These results confirm that the HA/PCL scaffold promotes the development of a more mature bone matrix compared to the PCL scaffold ($P < 0.01$, Figure 10b).

qRT-PCR analysis of cranial bone tissue further supported these histological findings. The expression levels of key osteogenic markers, including BMP2, OCN, and Runx2, were significantly elevated in the HA/PCL group compared to the PCL group ($P < 0.01$). These results suggest that the HA/PCL scaffolds not only enhance bone formation but also promote the upregulation of genes critical for osteogenic differentiation and bone regeneration (Figure 10c).

Discussion

Several studies have demonstrated that the porous structure of bionic bone scaffolds is advantageous for tissue ingrowth, nutrient and metabolite transport, and the long-term stability of bone material integration and implantation[14,15]. In this study, 3D printing was used to fabricate the HA/PCL scaffold. SEM imaging revealed the 3D porous structure of the scaffolds, with fibers arranged neatly and tightly connected. This 3D pore structure provides a larger space for cell adhesion, migration, and proliferation, while also offering a transport channel for nutrients and metabolites, facilitating cell growth and metabolism within the scaffold. Traditional methods of fabricating bionic bone scaffolds cannot achieve precise microstructural control, resulting in limited ability to manage the mechanical and biological properties of the materials[16]. In contrast, 3D printing allows for accurate control over the scaffold's 3D structure. Fused deposition modeling, a commonly used 3D printing technique, deposits thermoplastic material layer by layer using a temperature-controlled moving nozzle to build 3D structures. Additionally, it has been widely adopted as a production method for synthetic scaffolds[17,18].

We characterized the physicochemical properties of the HA/PCL 3D bionic porous bone scaffold prepared by 3D printing. The average pore size of the scaffolds in this study was 462.00 ± 100.389 μm, which falls within the 400 μm–600 μm range typically considered optimal for cell growth, as reported by most current studies. Increased porosity has been shown to enhance bone induction and improve cell attachment to the scaffold, as porosity determines the available surface area for cell-scaffold interactions. Scaffolds with porosity between 35% and 75% promote cell adhesion and growth, while 40%–60% porosity facilitates the diffusion and flow of cells and nutrients[19]. The porosity of human cancellous bone ranges from 50% to 90%[20]. In this study, the scaffolds exhibited a porosity of 53%, which is conducive to promoting cell proliferation. The balance between surface hydrophilicity

and hydrophobicity is a key factor influencing the cell compatibility of biomaterials. Hydrophilicity, in particular, plays a crucial role in cell adhesion and proliferation, while also impacting scaffold degradation[21-24]. To optimize both degradation performance and mechanical properties, PCL was incorporated into the scaffolds. The average contact angle of the scaffolds was slightly above 90°, indicating a superior hydrophilicity compared to pure PCL scaffolds. For bone tissue engineering scaffolds to function effectively, they must withstand certain loads to provide space for cell adhesion and proliferation[25]. The ideal mechanical properties of bone tissue engineering scaffolds aim to replicate those of natural bone tissue[26,27]. The Young's modulus of human cancellous bone is approximately 50 MPa, with compressive strength ranging from 7 to 10 MPa[28]. The scaffolds in this study demonstrated a Young's modulus of 53.82 MPa and compressive strength of 6.10 MPa, which, while not matching the mechanical properties of human cortical bone, align with the characteristics of adult cancellous bone.

Seed cells play a crucial role in bone tissue engineering[29]. In this study, BMSCs and VEPCs were selected as seed cells. After two weeks of cell culture on the scaffold material, the growth of BMSCs and VEPCs was significantly better compared to cells without scaffold loading. CCK-8 assay results further demonstrated that the cells proliferated well when loaded into the scaffold, with the mixed cells exhibiting enhanced proliferation. Additionally, the HA/PCL bionic porous bone scaffolds displayed no cytotoxicity and showed good biological compatibility. The osteogenic differentiation ability of the cells was significantly enhanced after scaffold loading, with the mixed cells showing the strongest osteogenic differentiation among all groups. These findings suggest that the two cell types mutually promote osteogenic differentiation on the scaffold, highlighting the potential for optimizing scaffold performance.

ALP is an early marker of osteogenic differentiation, and its elevated activity indicates active osteoblast function[30]. Co-culturing BMSCs and VEPCs with the HA/PCL scaffold significantly increased ALP activity, particularly in the mixed cell + scaffold group, suggesting a synergistic effect. qRT-PCR results further confirmed high expression of osteogenic genes (BMP2, OCN, Runx2) in this group, supporting enhanced osteogenesis. These findings indicate that the HA/PCL scaffold not only supports cell proliferation but also promotes bone regeneration[31,32]. H&E and Masson's trichrome staining revealed more extensive new bone formation and collagen deposition in the HA/PCL group compared to the PCL group, suggesting that hydroxyapatite enhances bone regeneration. However, complete defect repair was not achieved, emphasizing the need for further optimization of the scaffold. qRT-PCR results also demonstrated enhanced expression of osteogenic markers, underscoring the scaffold's bioactivity and its potential for improving bone regeneration.

These *in vitro* and *in vivo* experimental results collectively demonstrate the excellent potential of HA/PCL scaffold materials in bone tissue engineering. Future studies could focus on optimizing scaffold designs for clinical applications or integrating growth factors and drugs to enhance repair outcomes. Additionally, the limitations of this study, such as the comparison between animal model bone defects and human bone defects, as well as the need for longer follow-up periods to assess long-term integration and functional recovery of the newly formed bone, should be addressed.

The HA/PCL 3D-printed scaffold shows promising potential for bone tissue engineering by promoting osteogenic differentiation and bone regeneration both *in vitro* and *in vivo*. Its biocompatibility and ability to support the proliferation and differentiation of BMSCs and VEPCs suggest its suitability for bone repair applications. However, further optimization is required to address large bone defects fully. This study offers a basis for future research to improve scaffold design and explore its potential clinical applications in bone tissue engineering.

Conclusion

The mechanical and chemical properties of the HA/PCL 3D bionic porous bone scaffold prepared through 3D printing demonstrate its potential to mimic the characteristics of human cancellous bone. Following cell culture, the HA/PCL 3D scaffold shows no toxicity and exhibits good biological compatibility. When loaded with BMSCs and VEPCs, the HA/PCL scaffold promotes the best osteogenic differentiation both *in vitro* and *in vivo*, making it suitable for optimal bone tissue engineering scaffold design. Further research and clinical studies are needed to explore its full potential.

Ethics approval

All experimental procedures were approved by the Animal Care and Use Committee of Southwest Medical University (Ethics Approval Number: 20201185) and adhered to the National Institutes of Health (NIH) guidelines for the care and use of laboratory animals.

Authors' Contributions

Shi Shen, Benchao Shu, and Naiqiang Zhuo conceived and designed the study. They also conducted the study. Yulin Xu and Heng Zhao contributed to data acquisition and interpreted the data. Yang Li, Yujie Li, and Chuanchuan Zhuo analyzed the data. Shi Shen, Benchao Shu, and Naiqiang Zhuo drafted and revised the manuscript. All authors read and approved the final version of the manuscript.

Funding

This study was supported by the Luzhou – Southwest Medical University Joint Project (2020LZXNYDJ06), the Southwest Medical University university-level project (2019ZQN094), and the PhD Scientific Research Start-up Fund of the Affiliated Hospital of Southwest Medical University (18114).

References

1. Sohn HS, Oh JK. Review of bone graft and bone substitutes with an emphasis on fracture surgeries. Biomater Res 2019;23:9.
2. Gillman CE, Jayasuriya AC. FDA-approved bone grafts and bone graft substitute devices in bone regeneration.

Mater Sci Eng C Mater Biol Appl 2021;130:112466.
3. Xue N, Ding X, Huang R, Jiang R, Huang H, Pan X, Min W, Chen J, Duan JA, Liu P, Wang Y. Bone Tissue Engineering in the Treatment of Bone Defects. Pharmaceuticals (Basel) 2022;15(7):879.
4. Huang Q, Xu YB, Ren C, Li M, Zhang CC, Liu L, Wang Q, Lu Y, Lin H, Li Z, Xue HZ, Zhang K, Ma T. Bone transport combined with bone graft and internal fixation versus simple bone transport in the treatment of large bone defects of lower limbs after trauma. BMC Musculoskelet Disord 2022;23(1):157.
5. Han W, Shen J, Wu H, Yu S, Fu J, Xie Z. Induced membrane technique: Advances in the management of bone defects. Int J Surg 2017;42:110-116.
6. Feng Y, Zhu S, Mei D, Li J, Zhang J, Yang S, Guan S. Application of 3D Printing Technology in Bone Tissue Engineering: A Review. Curr Drug Deliv 2021;18(7):847-861.
7. Holzapfel BM, Rudert M, Hutmacher DW. Gerüstträgerbasiertes Knochen-Tissue-Engineering [Scaffold-based Bone Tissue Engineering]. Orthopade 2017;46(8):701-710.
8. Wubneh A, Tsekoura EK, Ayranci C, Uludağ H. Current state of fabrication technologies and materials for bone tissue engineering. Acta Biomater 2018;80:1-30.
9. Boskey AL, Roy R. Cell culture systems for studies of bone and tooth mineralization. Chem Rev 2008;108(11):4716-33.
10. Wang X, Wang Y, Gou W, Lu Q, Peng J, Lu S. Role of mesenchymal stem cells in bone regeneration and fracture repair: a review. Int Orthop. 2013;37(12):2491-8.
11. Jiao Z, Luo B, Xiang S, Ma H, Yu Y, Yang W. 3D printing of HA / PCL composite tissue engineering scaffolds. Advanced Industrial and Engineering Polymer Research. 2019;2(4):196-202. https://doi.org/10.1016/j.aiepr.2019.09.003.
12. Murugan S, Parcha SR. Fabrication techniques involved in developing the composite scaffolds PCL/HA nanoparticles for bone tissue engineering applications. J Mater Sci Mater Med 2021;32(8):93.
13. Wang F, Tankus EB, Santarella F, Rohr N, Sharma N, Märtin S, Michalscheck M, Maintz M, Cao S, Thieringer FM. Fabrication and Characterization of PCL/HA Filament as a 3D Printing Material Using Thermal Extrusion Technology for Bone Tissue Engineering. Polymers (Basel) 2022;14(4):669.
14. Abbasi N, Hamlet S, Love RM, Nguyen NT. Porous scaffolds for bone regeneration. Journal of Science: Advanced Materials and Devices 2020;5(1):1-9.
15. Collins MN, Ren G, Young KW, Pina S, Reis RL, Oliveira JM. Scaffold Fabrication Technologies and Structure/Function Properties in Bone Tissue Engineering. Advanced Functional Materials 2021;31(21):2010609.
16. Zhou C, Deng C, Chen X, Zhao X, Chen Y, Fan Y, Zhang X. Mechanical and biological properties of the micro-/nano-grain functionally graded hydroxyapatite bioceramics for bone tissue engineering. J Mech Behav Biomed Mater 2015;48:1-11.
17. Zein I, Hutmacher DW, Tan KC, Teoh SH. Fused deposition modeling of novel scaffold architectures for tissue engineering applications. Biomaterials 2002;23(4):1169-85.
18. Do AV, Khorsand B, Geary SM, Salem AK. 3D Printing of Scaffolds for Tissue Regeneration Applications. Adv Healthc Mater 2015;4(12):1742-62.
19. Will J, Melcher R, Treul C, Travitzky N, Kneser U, Polykandriotis E, Horch R, Greil P. Porous ceramic bone scaffolds for vascularized bone tissue regeneration. J Mater Sci Mater Med 2008;19(8):2781-90.
20. Zhang Y, Ahn PB, Fitzpatrick DC, Heiner AD, Poggie RA, Brown TD. Interfacial frictional behavior: cancellous bone, cortical bone, and a novel porous tantalum biomaterial. J Musculoskeletal Res 1999;3(04):245-251.
21. Gao JC, Chen S, Tang D, Jiang L, Shi J, Wang S. Mechanical Properties and Degradability of Electrospun PCL/PLGA Blended Scaffolds as Vascular Grafts. Transactions of Tianjin University 2018;25(2):152-160.
22. Nishida M, Tanaka T, Hayakawa Y, Ogura T, Ito Y, Nishida M. Multi-scale instrumental analyses of plasticized polyhydroxyalkanoates (PHA) blended with polycaprolactone (PCL) and the effects of crosslinkers and graft copolymers. RSC Adv 2019;9(3):1551-1561.
23. Thomas P. Influence of MnCl 2 on the properties of an amino acid complex single crystal- l -arginine perchlorate (LAPCl) for optical limiter applications. Journal of Materials Science: Materials in Electronics 2019;30(9):8407-8421.
24. Shi X, Wang Y, Ren L, Lai C, Gong Y, Wang DA. A novel hydrophilic poly(lactide-co-glycolide)/lecithin hybrid microspheres sintered scaffold for bone repair. J Biomed Mater Res A 2010;92(3):963-72.
25. Li Y, Zhou J, Hu S, Wang J, Wang K, Wang W. [Methods of improving the mechanical properties of hydrogels and their research progress in bone tissue engineering]. Zhongguo Xiu Fu Chong Jian Wai Ke Za Zhi 2021;35(12):1615-1622.
26. Aldemir BA, Dikici S, Öztürk Ş, Kahraman O, Ürkmez AŞ, Oflaz H. 3D Tissue Scaffold Printing On Custom Artificial Bone Applications. Süleyman Demirel Üniversitesi Fen Bilimleri Enstitüsü Dergisi 2015;18(3):1-9.
27. Torres FG, Nazhat SN, Sheikh Md Fadzullah SH, Maquet V, Boccaccini AR. Mechanical properties and bioactivity of porous PLGA/TiO2 nanoparticle-filled composites for tissue engineering scaffolds. Composites science and technology 2007;67(6):1139-1147.
28. Kumar A, Mandal S, Barui S, Vasireddi R, Gbureck U, Gelinsky M, Basu B. Low temperature additive manufacturing of three dimensional scaffolds for bone-tissue engineering applications: Processing related challenges and property assessment. Materials Science and Engineering: R: Reports 2016;103:1-39.
29. Shi R, Huang Y, Ma C, Wu C, Tian W. Current advances

for bone regeneration based on tissue engineering strategies. Front Med 2019;13(2):160-188.
30. Ansari S, Ito K, Hofmann S. Alkaline Phosphatase Activity of Serum Affects Osteogenic Differentiation Cultures. ACS Omega 2022;7(15):12724-12733.
31. Li J, Hao L, Wu J, Zhang J, Su J. Linarin promotes osteogenic differentiation by activating the BMP-2/RUNX2 pathway via protein kinase A signaling. Int J Mol Med 2016;37(4):901-10.
32. Hwang YJ, Hwang HJ, Go H, Park N, Hwang KA. Sword Bean (Canavalia gladiata) Pods Induce Differentiation in MC3T3-E1 Osteoblast Cells by Activating the BMP2/SMAD/RUNX2 Pathway. Nutrients 2023; 15(20):4372.